An AI-Based Pareto-Driven Cost-Dimension Optimization of EMI filters for DC-DC Converters

(Article begins on next page)

An AI-Based Pareto-Driven Cost-Dimension Optimization of EMI filters for DC-DC Converters

Lorenzo Nikiforos *, Francesco Gabriele *, Fabio Pareschi *,‡, Gianluca Setti §,‡

* DET – Politecnico of Torino, corso Duca degli Abruzzi 24, 10129 Torino, Italy.

email: {lorenzo.nikiforos, francesco.gabriele, fabio.pareschi}@polito.it

‡ ARCES – University of Bologna, via Toffano 2/2, 40125 Bologna, Italy.

§ CEMSE, King Abdullah University of Science and Technology (KAUST), Saudi Arabia. email: gianluca.setti@kaust.edu.sa

***Abstract*—This paper presents an AI-based and data-oriented optimization algorithm for the synthesis of passive Electro-Magnetic Interference (EMI) filters in DC–DC converters. The algorithm minimizes both cost and occupied area (or volume) targeting specific EMI attenuation levels and ensuring system stability. It operates on commercial component datasets and exploits the mathematical properties of Pareto dominance to explore feasible design configurations. Through dominance preserving set operators, the proposed approach guarantees exact Pareto-optimality while drastically reducing computational complexity. A neural network assists the optimization process by identifying computationally feasible ranges of component parameters, thus accelerating convergence. The method is validated on two commercial DC–DC converter evaluation boards from STMicroelectronics and Texas Instruments. It demonstrates its ability to identify solutions that outperform existing reference designs in both cost and area/volume.**

***Index Terms*—DC-DC converters, EMI Filters, Pareto front, Multi-Objective Optimization, Knapsack Problem, Neural Network, Artificial Intelligence**

I. Introduction

Switching-mode DC-DC converters are sources of conducted ElectroMagnetic Interference (EMI), potentially triggering malfunctions in devices operating within the same environment and leading to non-compliance with ElectroMagnetic Compatibility (EMC) regulations [1]. Passive EMI filters are broadly regarded as the most reliable and straightforward solution to attenuate conducted EMI [1]–[3]. As shown in Fig. 1, these are interposed between the DC-DC converter and the unregulated input voltage source, preventing the propagation of the current disturbance generated by the DC-DC converter to the input source. Nevertheless, passive EMI filters are generally expensive and bulky, potentially conflicting with overall manufacturing cost and occupied area (or volume) constraints [4]–[7]. As a consequence, developing cost- and area-effective passive EMI filters that ensure EMC compliance is a crucial aspect of modern power electronics design.

Previous studies in the literature addressed the optimization of passive EMI filters considering commercially available components. Different strategies have been explored, ranging from *a posteriori* generating method [8], evolutionary and heuristic algorithms [9]–[12] to machine learning–based [13] approaches, aiming to minimize costs and occupied area or volume while ensuring EMC. However, to the best of the authors' knowledge, the methods proposed in the literature either do not account for realistic commercial components or overlook costs and area/volume of the commercial components as primary optimization objectives. In this paper, we propose a novel Neural Network (NN)-based optimization algorithm grounded on the formal properties of Pareto dominance. The algorithm leverages on up-to-date commercial component datasets, synthesizing the Pareto-optimized set of passive EMI filters with respect to cost and area (or volume). Furthermore, a NN is employed to identify computationally feasible ranges of input components, ensuring a fast and efficient execution of the optimization algorithm.

The remainder of this paper is organized as follows. Section II reviews the key design aspects of passive EMI filters for DC–DC converters. In Section III, the proposed optimization methodology for the synthesis of Pareto-optimal EMI filter configurations is presented. The validity of the proposed optimization algorithm is demonstrated in Sec. IV, by considering two real case studies. Finally, we draw the conclusion.

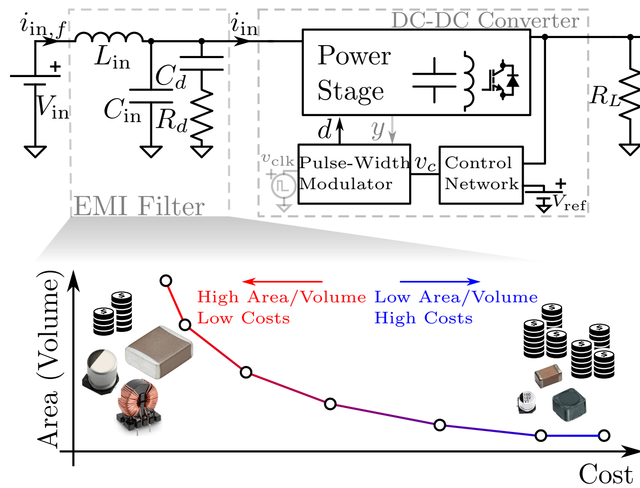

Fig. 1. An LC passive EMI filter employed for pulse-width modulated DC-DC converters and its cost and area (or volume) Pareto front optimization.

II. Design of Passive EMI Filters for DC-DC Converters

A. DC-DC converter Architecture Overview

A high-level view of closed-loop DC-DC converters is shown in Fig. 1. It includes the Power Stage (PS), the Control Network (CN) and the Pulse-Width Modulator (PWM). The PS includes the power semiconductor switches (e.g., Silicon Carbide MOSFETs, Gallium Nitride FETs), magnetic elements (e.g., inductor and transformer) and capacitors. In Fig. 1, the PS block represents a generic power conversion topology, thus covering both fundamental architectures (such as the Buck, the Boost and the Buck-Boost) and more advanced ones (e.g., Zeta, Sepic and Ćuk) [2]. In general, the PS produces a DC voltage v_{out} at its output port, to which the resistive load R_L is connected. The adopted CN ensures that the v_{out} is tightly regulated to the desired target value $V_{\mathrm{out}}^{\mathrm{target}}$. It is designed to guarantee system stability and achieve adequate transient performance. The CN takes as inputs the v_{out} and the reference input voltage V_{ref}, producing the control signal v_c as output. The signal v_c serves as input to the PWM stage, that in turn synthesizes the pulse-width modulated driving signal d. In fixed-frequency DC-DC converter control architecture, such as Voltage Mode Control (VMC) or Peak Current Mode Control (PCMC) [14], [15], a reference clock signal v_{clk} is provided to the PWM stage. In consequence, the signals q and v_{clk} are synchronized, as they both oscillate at the switching frequency f_{sw}. In order to further improve the converter performances, additional signals y can be sensed from the PS and fed to the PWM (e.g., the inductor current in PCMC).

B. The Design of a Passive Input EMI Filter

The input EMI filter topology considered in this work is the single-stage LC filter shown in Fig.1. It is connected between the DC input voltage source V_{in} and the Buck converter input port. This allows smoothing out the sharp transients of the converter input current i_{in}, thereby preventing their propagation back to the input source, thus mitigating EMI. The resulting filtered current is $i_{\mathrm{in},f}$. The EMI filter circuit network includes both the filtering elements L_{in} and C_{in} and the damping branch R_d-C_d. In practical scenarios, the damping branch does not have any impact on the high-frequency attenuation of the filter [2], [5]. Therefore, the attenuation imposed by the EMI filter can be quantified through the transfer function

$$H_f(s) = \frac{i_{\mathrm{in},f}(s)}{i_{\mathrm{in}}(s)} = \frac{1}{1+(\frac{s}{\omega_0})^2}, \tag{1}$$

where s is the complex Laplace variable and $\omega_0 = 1/\sqrt{L_{\mathrm{in}}C_{\mathrm{in}}}$. The attenuation imposed by the filter at f_{sw} is defined as $A_{\mathrm{sw}} = |H_f(s = \mathrm{j}2\pi f_{\mathrm{sw}})|$, where $|\cdot|$ denote, hereinafter, the magnitude operator. Since in practical design scenario $\omega_0 \ll 2\pi f_{\mathrm{sw}}$, it is possible to derive the simplified expression

$$A_{f_{\mathrm{sw}}} = \left(\frac{\omega_0}{2\pi f_{\mathrm{sw}}}\right)^2. \tag{2}$$

The damping elements R_d-C_d have a decisive role in guaranteeing system stability [2], [5]–[7]. In general, the stability boundaries of a closed-loop DC–DC converter in presence of an EMI filter can be evaluated from the minor loop gain $T_m(s) = Z_{\mathrm{out}}^{\mathrm{EMI}}(s)/Z_{\mathrm{in}}^{\mathrm{DC-DC}}(s)$, where $Z_{\mathrm{out}}^{\mathrm{EMI}}(s)$ is the EMI filter output impedance and $Z_{\mathrm{in}}^{\mathrm{DC-DC}}(s)$ is the closed-loop input impedance of the DC-DC converter [2]. For the sake of conciseness, we hereinafter specifically focus on the DC-DC Buck converter, serving as the basis for the subsequent application examples. In this case, the closed-loop input impedance is defined by the incremental negative resistance [2]

$$Z_{\mathrm{in}}^{\mathrm{DC-DC}}(s) = Z_{\mathrm{in}}^{\mathrm{Buck}} \approx \frac{R_L}{M^2}, \tag{3}$$

where $M = V_{\mathrm{out}}^{\mathrm{target}}/V_{\mathrm{in}}$. In this scenario, system stability is guaranteed if $|Z_{\mathrm{out}}^{\mathrm{EMI}}(s)| < |Z_{\mathrm{in}}^{\mathrm{Buck}}(s)|$. As a result, the elements R_d-C_d are designed to damp the peak of $|Z_{\mathrm{out}}^{\mathrm{EMI}}(s)|$. By defining $n = C_d/C_f$, optimum component values for the damping network are given by the expressions [2]

$$\begin{aligned} n &> \left(\frac{R_{0,f}^2}{\left|Z_{\mathrm{in}}^{\mathrm{Buck}}\right|}\right)^2 \left(1+\sqrt{1+\left(2\frac{\left|Z_{\mathrm{in}}^{\mathrm{Buck}}\right|}{R_{0,f}}\right)^2}\right) \\ R_d &= R_{0,f}\sqrt{\frac{(2+n)(4+3n)}{2n^2(4+n)}}, \end{aligned} \tag{4}$$

where $R_{0,f} = \sqrt{L_f/C_f}$. Accordingly, as a result, the elements L_{in} and C_{in} are designed via (2) to meet the imposed EMI attenuation performances, while (4) defines the R_d-C_d component values to ensure system stability [2].

III. The Developed Optimization Algorithm

The proposed algorithm produces feasible and optimized EMI filter designs based on a dataset generated from commercial component distributor's website. In particular, it permits to derive the Pareto set of achievable trade-offs between area a (or volume t) and cost c, subject to electrical feasibility constraints. To reduce the overall computational cost, a NN is employed prior to executing the proposed algorithm to preselect a relevant subset of components from the developed dataset.

A. Dataset Generation and Preliminary Considerations

The dataset $\mathcal{D}$ is generated by selecting commercial components from the distributor's website Mouser Electronics [16]. The components are selected from the website in order to satisfy practical design constraints, e.g., coil saturation current, rated voltage and current values and temperature operating ranges. Each element of $\mathcal{D}$ is associated to an available commercial component and it embeds the information a (or t), c and nominal value v. It should be noted that for a given v, the dataset $\mathcal{D}$ contains multiple commercial component parts with different a (or t) and c.

In the remainder of the article, the following definitions are adopted. We indicate with $\mathcal{I}_{\mathrm{Cap}}$, $\mathcal{I}_{\mathrm{Ind}}$ and $\mathcal{I}_{\mathrm{Damp}}$ the sub-datasets extracted from $\mathcal{D}$ respectively for the filtering capacitors, the filtering inductors and the damping capacitors. Each element of the sub-datasets is a triple (v, a, c), that are respectively the nominal value, the area and the cost of the element. Furthermore, we define the sets $\mathcal{Z}_\alpha^\beta = \{(a, c) \mid (v, a, c) \in \mathcal{I}_\alpha : v = \beta\}$, where $\alpha \in \{\mathrm{Cap}, \mathrm{Ind}, \mathrm{Damp}\}$ and $\beta \in \{C_f, L_{\mathrm{in}}, C_d\}$. The same definitions apply when a is directly replaced by t.

In order to move toward the practical realization of the EMI filter topology shown in Fig. 1, the final Pareto set obtained by the proposed optimization procedure only includes solutions that selects from $\mathcal{D}$ a single inductor of value L_{in}, a single damping capacitor of value C_d, and multiple filtering capacitors C_f connected in parallel to obtain an overall capacitance of value C_{in}.

B. Fundamental set Operators and Dominance Preservation

We recall here the concepts of Pareto set and dominance. Then, we define the fundamental set operators employed by the proposed algorithm and their proprieties. Let $\mathcal{S} = \{S_0, ..., S_N\}$, where $S_i \subset \mathbb{R}^2$, $\forall i \in \{1, 2, ..., N\}$.

Dominance: Let the points $p_0 = (x_0, y_0)$ and $p_1 = (x_1, y_1)$, where $p_0, p_1 \in S_i$, where $S_i \in \mathcal{S}$. We say that p_0 *dominates* p_1, here denoted $p_0 \prec p_1$, if $x_0 \leq x_1$, $y_0 \leq y_1$, and at least one inequality is strict.

Pareto Set and Operator: The Pareto set (or Pareto front) of $S_i \in \mathcal{S}$ is defined as

$$P(S_i) = \{p_k \in S_i \mid \nexists\, p_n \in S_i : p_n \prec p_k\}. \tag{5}$$

Therefore, we implicitly define the Pareto operator $P(\cdot)$, mapping the set S_i to its Pareto front, by removing dominated points.

Aggregation: given $S_i, S_j \in \mathcal{S}$, we define the aggregation operator as $\mathcal{A}(S_i, S_j) := \{(x_k + x_v, y_k + y_v) \mid p_k = (x_k, y_k) \in S_i, p_v = (x_v, y_v) \in S_j\}$. This operator produces all componentwise sums of points in S_i and S_j.

Union: $\mathcal{U}(\mathcal{S})$: collects all points from the sets, i.e., $\bigcup_{k=1}^N S_k$.
If the output of the operators $\mathcal{A}, \mathcal{U}$ is restricted to be a Pareto front, then it is safe to replace each input set by its Pareto reduction. This is formally demonstrated below but intuitively, dominated points cannot contribute to non-dominated outcomes after aggregation or union. Fig. 2 graphically shows this.

Lemma 1: The Pareto front remains invariant to prior Pareto reduction of the aggregated sets. Let $S_i, S_j \in \mathcal{S}$, then

$$P(\mathcal{A}(S_i, S_j)) = P(\mathcal{A}(P(S_i), P(S_j))). \tag{6}$$

Proof: Without loss of generality, we provide the proof for the set S_i only. Let $p_k = (x_k, y_k) \in S_i$ be dominated by $p'_k = (x'_k, y'_k) \in P(S_i)$ and $p_v = (x_v, y_v) \in S_j$. Since $p'_k \prec p_k$, then

$$(x'_k + x_v,\ y'_k + y_v) \prec (x_k + x_v,\ y_k + y_v).$$

Hence, dominated points in S_i cannot generate non-dominated outcomes after aggregation. Therefore, only points in $P(S_i)$ could contribute to generating the points in $P(\mathcal{A}(S_i, S_j))$. □

Lemma 2: The Pareto front is invariant to prior Pareto reduction of the united sets:

$$P(\mathcal{U}(\mathcal{S})) = P(\mathcal{U}(\{P(S_1), P(S_2), ...P(S_i), ..., P(S_N)\})) \tag{7}$$

Proof: Without loss of generality, we provide the proof for the set S_i only. If a point $p_k \in S_i$ is dominated within its own set, then there exists another point $p_v \in S_i$ such that $p_v \prec p_k$. Since $S_i \subseteq \bigcup_{k=1}^N S_k$, the same domination relation holds in the union. Therefore, points that are not in $P(S_i)$ do not appear in the final Pareto front $P(\mathcal{U}(\mathcal{S}))$. □

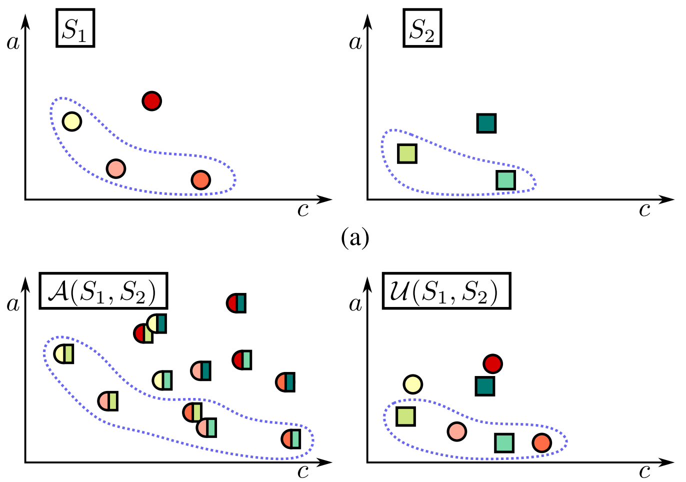

Fig. 2. Illustration of the set operators. (a) Two sets, S_1 and S_2, are represented in the objective space of area versus cost. (b) The sets are combined using the aggregation operator $\mathcal{A}(S_1, S_2)$, and the union operator $\mathcal{U}(S_1, S_2)$. The blue dashed curves group the points representing the Pareto fronts in each plot. Note that points not on the Pareto front of S_1 or S_2 cannot contribute to non-dominated points after applying either the aggregation or union operators.

Algorithm 1 Pareto-optimal Filter Synthesis.

For each nominal value C_f, L_{in} and C_{d}, compute $P(\mathcal{Z}_{\text{Cap}}^{C_f})$, $P(\mathcal{Z}_{\text{Ind}}^{L_{\text{in}}})$ and $P(\mathcal{Z}_{\text{Damp}}^{C_d})$.
Construct DP$[C_{\text{in}}]$ for all the possible value of C_{in}.
Initialize final front: $F \leftarrow \emptyset$
for all L_{in} **do**
    for all C_{in} **do**
        if Constraint(L_{in}, C_{in}) is satisfied **then**
            Initialize set: $I \leftarrow \emptyset$
            for all C_d **do**
                if Constraint(L_{in}, C_{in}, C_{d}) is satisfied **then**
                    Append $P(\mathcal{Z}_{\text{Damp}}^{C_d})$ to I
                end if
            end for
            $I \leftarrow P(\mathcal{U}(I))$
            Append $P(\mathcal{A}(\mathcal{A}(\text{DP}[C_{\text{in}}], P(\mathcal{Z}_{\text{Ind}}^{L_{\text{in}}})), I))$ to F
        end if
    end for
end for
$F \leftarrow P(\mathcal{U}(F))$

	f_{sw}[kHz]	$V_{\text{in}}^{\min}$[V]	$V_{\text{out}}^{\text{target}}$[V]	$I_{\text{out}}^{\max}$[A]	$R_L^{\min}[\Omega]$
STEVAL-L3751V12	230	6	5	15	1.2
LM25149-Q1EVM-2100	2100	5.5	5	8	0.625

TABLE I
PARAMETER VALUES OF THE CONSIDERED DC-DC BUCK CONVERTERS.

C. Proposed Optimization Algorithm and Implementation

The proposed optimization algorithm exploits the component dataset generated as described in III-A, producing as the final output the Pareto front of feasible passive EMI filter realizations satisfying given attenuation and stability constraints defined in (2) and (4), respectively.

The implementation of the optimization method is shown via the Algorithm 1. As will become evident from the discussion below, the algorithm uniquely resorts to the $\mathcal{A}$ and $\mathcal{U}$ operators. Moreover, since its final output is a Pareto front Lemmas 1 and 2 guarantee that only Pareto sets need to be retained at each stage. Therefore, it is worth observing that *i)* for each nominal component value, it is sufficient to store the Pareto-optimal area and cost pairs and *ii)* this translate in implementing just the right-side members of (7) and (6), respectively for the $\mathcal{U}$ and $\mathcal{A}$ operators, enabling a computationally-efficient implementation of the algorithm. For the implementation of $\mathcal{U}$, the sets are merged pairwise using a two-pointer technique, analogous to the merge phase of a merge sort algorithm. If each input front is sorted by cost, the two-pointer traversal efficiently producing their combined Pareto front in linear time. For this reason we always keep Pareto front sorted by cost. The merge procedure is then applied recursively until a single final Pareto front remains. The implementation of $\mathcal{A}$ exploits an incremental approach, that is adopted to speed up calculation. Specifically, referring to the definition of the $\mathcal{A}$ operator in Sec. III-B, for each point $p_v \in S_j$, the set S_i is translated by p_v, yielding an intermediate front $\mathcal{A}(S_i, \{p_v\})$. These intermediate fronts are then merged recursively exploiting the $\mathcal{U}$ operation described above. All these considerations allow substantial reduction of the computational burden without loss of accuracy.

Having explained the implementation of the operators $\mathcal{A}$ and $\mathcal{U}$, we now detail the derivation of the nominal value C_{in}. This process relies on exploring all the possible combination of all the available capacitors with nominal C_{f}, together with their relative cost and area. In practice, from the design relations defined in (2) and (4) it follows that after choosing the values L_{in} and C_d, the feasible value of C_{in} must satisfy

$$C_{\text{in}} \geq \max\left(\frac{1}{4\pi^2 L_{\text{in}} A_{f_{\text{sw}}} f_{\text{sw}}^2}, \frac{4Z_{\min}^2 L_{\text{in}}^3}{C_d^2 - L_{\text{in}}^2}\right). \tag{8}$$

Since the available L_{in} and C_d values in $\mathcal{I}_{\text{Ind}}$ and $\mathcal{I}_{\text{Damp}}$ are discrete and bounded, there must always exist a value $\hat{C}_{\text{in}}$ satisfying (8) for every possible choice of L_{in} and C_d. Beyond this limit, any additional capacitance can always be removed without violating the constraint in (8), while strictly decreasing the total cost and area. Hence, by restricting the search to $C_{\text{in}} \leq \hat{C}_{\text{in}}$, all potentially optimal configurations are preserved avoiding unnecessary computations. The solution of this problem can be achieved using a dynamic programming algorithm similar to the one used for the unbounded knapsack problem [17].

Let DP $[C_{\text{in}}]$ denote the Pareto set of the (a, c) pairs for the total capacitance value C_{in}. For each available capacitance of nominal value C_f and its relative Pareto set $P\left(\mathcal{Z}_{\text{Cap}}^{C_f}\right)$, we update

$$\text{DP}\left[C_{\text{in}}\right] \leftarrow P\left(\mathcal{U}\left(\text{DP}[C_{\text{in}}], \mathcal{A}\left(\text{DP}[C_{\text{in}} - C_f], P\left(\mathcal{Z}_{\text{Cap}}^{C_f}\right)\right)\right)\right). \tag{9}$$

Furthermore, to reduce the computational cost, some of the solutions on the Pareto front are discarded. For each DP$[C_{\text{in}}]$, only K points are retained. These are selected to ensure an approximately uniform coverage of the original set. A distance-based heuristic is employed, which iteratively removes the point with the smallest inter-point distance, while ensuring that the extreme solutions are always preserved.

D. NN–Based Range Selection

The datasets of commercial filtering inductors and capacitors $\mathcal{I}_{\text{Cap}}$ and $\mathcal{I}_{\text{Ind}}$ can include a very large number of nominal component values. This results in a prohibitive computational burden, since the dynamic programming table must be generated for every possible combination of component values. To mitigate this issue, a NN–based selection stage has been introduced to restrict the ranges of the nominal values.

This procedure starts by retaining only M consecutive values of both filtering inductors and capacitors from a pair of pre-selected lower bounds $L_{\text{in}}^{\min}$ and $C_f^{\min}$. In consequence, the corresponding upper bounds are automatically defined by the M parameter, here

	Opt. Area - TI	Opt. Volume - TI	Opt. Area - STM	Opt. Volume - STM
$C_{\text{in}}^{\min}$	680 nF	680 nF	680 nF	470 nF
$L_{\text{in}}^{\min}$	360 nH	400 nH	8.6 µH	1.4 µH

TABLE II
RANGES SELECTED FOR THE TARGET EVALUATIONS.

	LM25149-Q1EVM-2100	Opt. Area - TI	Opt. Volume - TI	STEVAL-L3751V12	Opt. Area - STM	Opt. Volume - STM
L_{in}	744383560068	815-SPIAIGF4020.40MT	815-SPIAIGF4020.40MT	XAL5050-822MEC	994-XAL6060-103MEC	504-EXL1V0503-3R3-R
C_{in}	1x 12105C106K4Z2A 1x CNA6P1X7R1H106K250AE 2x UMK212BB7225KG-T	1x 63-MSASU168BB5225KT 4x 187-CL31B106KBHNNNE	1x 963-MSASU168BB5225KT 2x 187-CL31B106KBHNNNE 2x 81-GRM31CD71H106KE1K	10 x GRM32EC72A106KE05	1x 81-GRT21BD72A225KE13 8x 187-CL32Y106KCVZ4NE	64x 605-101S41W392KV4E
C_d	EEE-FK1H470P	598-HZA226M050D16T-F	598-HZA226M050D16T-F	VEJ101M2ATR-1313	661-MVH100V680M	71-MAL214297901E3

TABLE III

PART NUMBERS OF THE COMPONENTS EMPLOYED IN THE COMMERCIAL AND OPTIMIZED EMI FILTERS IMPLEMENTATION.

Layers	Activation Function	Loss	Optimizer	Momentum	Learning Rate	Weight Decay	Batch Size	Epochs	Accuracy
(61, 64, 64, 64, 64, 2)	ReLU	Cross-entropy	SGD	0.9	10^{-3}	10^{-4}	64	300	98.7%

TABLE IV

MULTILAYER PERCEPTRON TRAINING CONFIGURATION AND PERFORMANCE.

Algorithm 2 Heuristic employed in ranges selection.

Initialize $s \leftarrow 0$
for all $L_{\text{in}}^{\min} \leq L_{\text{in}} \leq L_{\text{in}}^{\max}$ **do**
  for all $C_{\text{f}}^{\min} \leq C_{\text{f}} \leq C_{\text{f}}^{\max}$ **do**
    Compute $x = \lceil 2\pi f_{\text{sw}} \sqrt{A_{f_{\text{sw}}}}/C_f L_{\text{in}} \rceil$
    Compute $z_1 \leftarrow \text{Mean}(P(\mathcal{Z}_{\text{Cap}}^{C_f}))$
    Compute $z_2 \leftarrow \text{Mean}(P(\mathcal{Z}_{\text{Ind}}^{L_{\text{in}}}))$
    Compute $p \leftarrow z_1 x + z_2$
    $s \leftarrow s + p[1] \cdot p[2]$
  end for
end for

denoted as $L_{\text{in}}^{\max}$ and $C_f^{\max}$. Then, the NN implements a binary classification, predicting whether for a given pair of C_f-L_{in} ranges would lead to an excessive computational effort. The selection and classification procedure is repeated for all the possible choices of lower-bounds starting from the component values available in the dataset. Among all the computationally feasible ranges, only a specific pair of inductor and capacitor intervals is finally chosen. This last step is carried out resorting to the simple heuristic Algorithm 2.

The training dataset of the NN is built by randomly selecting M component values among the ones available in the datasets $\mathcal{I}_{\text{Cap}}$ and $\mathcal{I}_{\text{Ind}}$. From these values, the optimization Algorithm 1 is simulated, and each simulation is labeled as computationally feasible or too expensive, according to the observed execution time based on an empirically chosen threshold. Overall, each entry of the dataset contains the chosen nominal component values together with the length of their associated Pareto fronts as inputs, and the correspondent label as the target output.

IV. THE EXAMINED CASE STUDY AND RESULTS

To validate the effectiveness of the proposed optimization algorithm, we focus on two case studies based on commercial DC-DC Buck converter applications. The first one considers the LM25149-Q1EVM-2100 evaluation board developed by Texas Instruments [15], integrating a PCMC Buck converter. The second case study examines the evaluation board STEVAL-L3751V12 developed by STMicroelectronics [14], embedding a VMC Buck converter. The main parameters of the converters are summarized in Table I. Both the evaluation boards include built-in passive EMI filters, whose component part numbers are mentioned in [15], [18] and referenced in Table III. By referring to the website of the electronic components distributor Mouser Electronics [16], it is possible to estimate both the overall occupied area/volume and costs of the implemented EMI filters. The total occupied area/volume and costs are obtained by directly summing the individual area/volume and cost contributions of the employed components in Table III.

The datasets of commercial components used by the optimization algorithm are built using the Mouser Electronics database. In order to make a fair comparison, the components are selected so that their main specifications are compatible with those of the components in [15], [18]. These include tolerance values, rated voltage/current values, saturation current values and operating temperature ranges.

The dataset employed for training the Neural Network is constructed by randomly retaining $M = 15$ values of inductance and capacitance from the original Mouser component database. For each

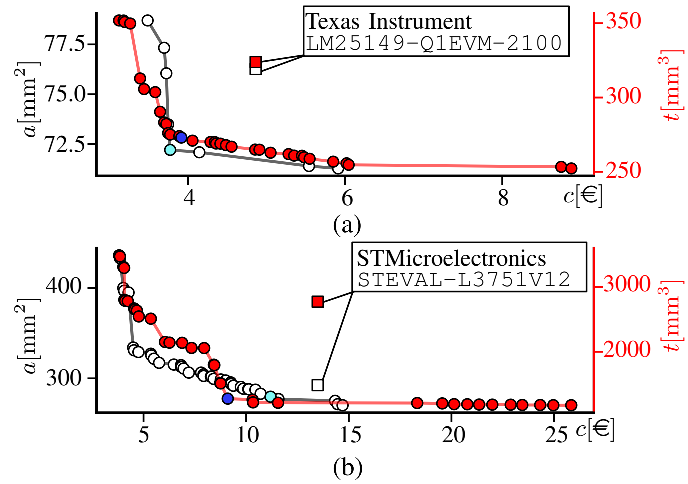

Fig. 3. Pareto fronts obtained for two case studies: (a) Texas Instruments LM25149-Q1EVM-2100 board and (b) STMicroelectronics STEVAL-L3751V12 board. The white dots represent the Pareto front for the total area, while the red dots correspond to the Pareto front for the total volume. The square markers indicate the reference evaluation boards. The light and dark blue dots highlight solutions that outperform the reference boards in both metrics, both considering the occupied area and volume.

sample, the optimization algorithm is executed to assess its computational feasibility. If the algorithm completed within the empirically chosen threshold level of 10^{11} operations, the sample is labeled as computationally feasible. Conversely, the process is terminated and the sample is labeled as computationally expensive. Overall, the training set consists of 19.200 samples, whereas the test set contains 3.400 samples. The implemented NN is a multilayer perceptron, whose training configuration and performances are summarized in Table IV. The selected ranges, summarized in Table II, are employed in the optimization process. The corresponding results are shown in Fig. 3. It is evident that the passive EMI filters implemented on both the evaluation boards are not located on the Pareto front. This indicates that there exist component choices that improve both optimization metrics simultaneously. An example of these solutions is highlighted by the light and dark blue dots in Fig. 3, whose corresponding part numbers of the commercial components are listed in Table III.

V. CONCLUSION

This paper proposes a Pareto-driven optimization framework for synthesizing passive EMI filters in DC–DC converters. The method efficiently explores discrete component datasets while rigorously preserving Pareto optimality through mathematically defined set operations. A NN is integrated into the proposed framework to effectively limit the search space of the optimization algorithm, thereby drastically reducing the overall computational cost. Validation on two commercial converter platforms demonstrates the capability of the proposed approach to identify solutions that outperform existing designs in both cost and area/volume.

REFERENCES

[1] C. R. Paul, *Conducted Emissions and Susceptibility*. John Wiley & Sons, Ltd, 2005.

[2] R. W. Erickson and D. Maksimovic, *Fundamentals of Power Electronics*, 3rd ed. Springer International Publishing, 2020.

[3] B. Narayanasamy and F. Luo, "A Survey of Active EMI Filters for Conducted EMI Noise Reduction in Power Electronic Converters," *IEEE Transactions on Electromagnetic Compatibility*, vol. 61, no. 6, pp. 2040–2049, 2019. doi: 10.1109/TEMC.2019.2953055

[4] N. Femia and G. Di Capua, "Optimum Design of Differential-Mode Input Filters for DC-DC Switching Regulators," in *2021 IEEE International Symposium on Circuits and Systems (ISCAS)*, 2021, pp. 1–5. doi: 10.1109/ISCAS51556.2021.9401400

[5] R. Erickson, "Optimal single resistors damping of input filters," in *APEC '99. Fourteenth Annual Applied Power Electronics Conference and Exposition. 1999 Conference Proceedings (Cat. No.99CH36285)*, vol. 2, 1999, pp. 1073–1079 vol.2. doi: 10.1109/APEC.1999.750502

[6] L. Xing, F. Feng, and J. Sun, "Optimal Damping of EMI Filter Input Impedance," *IEEE Transactions on Industry Applications*, vol. 47, no. 3, pp. 1432–1440, 2011. doi: 10.1109/TIA.2011.2127434

[7] L. Xing and J. Sun, "Optimal damping of multi-stage EMI filters," in *2011 Twenty-Sixth Annual IEEE Applied Power Electronics Conference and Exposition (APEC)*, 2011, pp. 1721–1728. doi: 10.1109/APEC.2011.5744828

[8] N. Hensgens, J. Oliver, J. A. Cobos, S. Skibin, and A. Ecklebe, "Design and multi-objective optimization of EMI input filters," in *2013 Twenty-Eighth Annual IEEE Applied Power Electronics Conference and Exposition (APEC)*, 2013, pp. 2506–2513. doi: 10.1109/APEC.2013.6520648

[9] X. Li, F. Lin, X. Zhang, M. Huang, and H. Wang, "Multi-objective Design of LC Filter for High-efficiency, High-power-density and High-performance Buck Converter," in *2019 IEEE Energy Conversion Congress and Exposition (ECCE)*, 2019, pp. 5132–5136. doi: 10.1109/ECCE.2019.8913162

[10] X. Li, X. Zhang, and F. Lin, "Multi-Objective Design of Output LC Filter for Buck Converter via the Coevolving-AMOSA Algorithm," *IEEE Access*, vol. 9, pp. 11 884–11 894, 2021. doi: 10.1109/ACCESS.2020.3034361

[11] G. Ala, G. Giglia, E. Francomano, M. Di Piazza, M. Luna, and G. Conte, "Design of EMI Filters Using Multi-Objective Optimization," in *2018 IEEE International Conference on Environment and Electrical Engineering and 2018 IEEE Industrial and Commercial Power Systems Europe (EEEIC / I&CPS Europe)*, 2018, pp. 1–5. doi: 10.1109/EEEIC.2018.8493746

[12] R. Orvai, J. Hamar, and M. Csörnyei, "A Practical Survey on Multi-Objective Optimization of EMI Filters," in *2025 International Symposium on Electromagnetic Compatibility – EMC Europe*, 2025, pp. 795–800. doi: 10.1109/EMCEurope61644.2025.11176335

[13] L. Zhang, H. Ge, Y. Ma, J. Xue, H. Li, and M. Pecht, "Multi-Objective Optimization Design of a Notch Filter Based on Improved NSGA-II for Conducted Emissions," *IEEE Access*, vol. 8, pp. 83 213–83 223, 2020. doi: 10.1109/ACCESS.2020.2991576

[14] STMicroelectronics, "STEVAL-L3751V12 Data Brief," https://www.st.com/resource/en/data_brief/steval-l3751v12.pdf, 2023, accessed: 2025-10-26.

[15] Texas Instruments Incorporated, "LM25149-Q1 EVM User's Guide," https://www.ti.com/lit/ug/snvu773a/snvu773a.pdf, 2022.

[16] Mouser Electronics, "Mouser Electronics Website," https://www.mouser.it/, Accessed: 26-Oct-2025.

[17] P. C. Gilmore and R. E. Gomory, "The Theory and Computation of Knapsack Functions," *Operations Research*, vol. 14, no. 6, pp. 1045–1074, Dec. 1966. doi: 10.1287/opre.14.6.1045. [Online]. Available: https://doi.org/10.1287/opre.14.6.1045

[18] STMicroelectronics, "STEVAL-L3751V12 Bill of Materials," https://www.st.com/resource/en/bill_of_materials/steval-l3751v12_bom.pdf, 2023, accessed: 2025-10-26.